

Time-Warping Invariant Quantum Recurrent Neural Networks via Quantum-Classical Adaptive Gating

Ivana Nikoloska¹, Osvaldo Simeone¹, Leonardo Banchi^{*2,3}, and Petar Velićković^{*4}

¹King's College London, Strand, London, WC2R 2LS, United Kingdom

²Department of Physics and Astronomy, University of Florence, via Sansone 1, I-50019, Sesto Fiorentino (FI), Italy

³INFN, Sezione di Firenze, via Sansone 1, I-50019, Sesto Fiorentino (FI), Italy

⁴DeepMind

Adaptive gating plays a key role in temporal data processing via classical recurrent neural networks (RNN), as it facilitates retention of past information necessary to predict the future, providing a mechanism that preserves invariance to time warping transformations. This paper builds on quantum recurrent neural networks (QRNNs), a dynamic model with quantum memory, to introduce a novel class of temporal data processing quantum models that preserve invariance to time-warping transformations of the (classical) input-output sequences. The model, referred to as *time warping-invariant QRNN (TWI-QRNN)*, augments a QRNN with a quantum-classical adaptive gating mechanism that chooses whether to apply a parameterized unitary transformation at each time step as a function of the past samples of the input sequence via a classical recurrent model. The TWI-QRNN model class is derived from first principles, and its capacity to successfully implement time-warping transformations is experimentally demonstrated on examples with classical or quantum dynamics.

1 Introduction

Sequential data is prevalent in both classical and quantum systems. Indeed, tasks like natural language processing [1, 2] or simulating the dynamics of quantum systems [3, 4] require computing architectures that are capable of capturing tem-

poral dependencies by retaining only the information about the past that is necessary to predict the future. This calls for *adaptive gating* mechanisms that can forget in a data-driven manner, so as to selectively memorize and overwrite information [5, 6].

For classical processes, it was recently formally proved that gating mechanisms ensure *invariance to time warping* [7, 8]. Consider, for example, monitoring vitals of patients in intensive care, or the evolution of a quantum system. Time-series data that result from these processes are not naturally discrete – they are in fact obtained by sampling a continuous signal. However, in practice, the sampling rate cannot always be controlled, and moreover, it may not always be fixed. Time warping transformations capture such dynamically changing sampling rates, or basic operations such as inserting a, possibly varying, number of zeros or white spaces between the elements of an input sequence. As such, time warping can model important practical aspects such as imperfect sampling due to jitter or clock drifts, or changes in time scales. Thereby, it is imperative to develop models that are immune to these transformations and are able to fit the corresponding “time-warped” signals.

Conventional recurrent neural networks (RNNs), which do not implement gating mechanisms, are not robust to time-warping transformations, failing even in simple settings with the additional of few zeros between samples [7]. In contrast, classical RNN models with gating, such as long short-term memories (LSTMs) and gated recurrent units (GRUs), can successfully adapt to transformed inputs. This paper aims at investigating quantum models that preserve time warping-invariance for temporal

^{*}alphabetical order

Ivana Nikoloska: ivana.nikoloska@kcl.ac.uk

data processing, targeting both classical and quantum dynamics.

1.1 Related Work

Reflecting the underlying symmetries of a given data set in the choice of the inductive bias is well known to be of fundamental importance for the success of classical machine learning. Whilst symmetries have always played an imperative role in studying physical systems and understanding the laws of physics, the study of symmetries in data has just recently gained momentum, leading to the blossoming field of geometric deep learning [8]. Symmetries formalize the invariance of objects under some set of operations. For example, the binding energy of a molecule does not change by permuting the order of the atoms, and a picture of a cat still depicts a cat regardless of the position of the cat within the image. Incorporating this prior knowledge into the learning architecture, as a geometric prior, e.g., by adopting a graph [9] or convolutional [10] neural network, has been shown to improve both trainability and generalization performance.

Recently, the quantum machine learning (QML) community has also focused on introducing geometric priors into quantum models [11, 12, 13]. For example, quantum graph neural networks preserve permutations symmetries, making them suitable for learning quantum tasks with a graph structure [14, 15, 16, 17]; whilst quantum convolutional neural networks [18] preserve translations symmetry. As their classical counterparts, symmetry-preserving quantum models have the potential not only of reducing sample complexity, but also to mitigate quantum computing-specific issues such as barren plateaus [19, 20].

A *quantum recurrent neural network* (QRNN) architecture that can successfully learn temporal dependencies using a repeat-until-success mechanism was first proposed in [21]. A separate QRNN model was later proposed in [22]. As illustrated in Fig. 1, a QRNN applies the same parametrized quantum circuit (PQC) sequentially over time, whilst retaining historical information in unmeasured “memory” qubits. The model has been shown to be capable of learning sequential data [22], and its capacity was analyzed in [23] in comparison to counterpart classical models with the same number of memory

units. In particular, it was shown in [24, 25] that quantum models can describe temporal sequences with reduced memory, compared to their classical counterparts. A model with classical memory, was introduced in [26] by integrating quantum models within a classical LSTM architecture. The latter model was also leveraged in [27] to define a reservoir computing solution with fixed dynamics. RNNs have also been integrated with quantum dynamical models in order to simulate non-Markovian dynamics in open system [28].

To the best of our knowledge, quantum models for temporal data processing have not yet been studied from the perspective of symmetry preservation. In this paper, we address this knowledge gap by focusing on models with quantum memory. To this end, we take the QRNN model in [22] as foundation due to its efficiency, although the general approach presented here could be extended to any quantum model with a recurrent structure.

1.2 Contribution

Inspired by the connection between gating and time warping unveiled in [7], in this paper we investigate the problem of preserving symmetries caused by time-warping transformations in quantum dynamic models. The main contributions are as follows.

- We introduce the class of *time warping-invariant QRNNs (TWI-QRNNs)*, which augment QRNNs with a *quantum-classical adaptive gating* mechanism that chooses whether to apply a parameterized unitary transformation or not at each time step as a function of the past samples of the input sequence via a classical recurrent model.
- The TWI-QRNN model class is derived from first principles via a postulate of invariance to time warping.
- While the TWI-QRNN model class implements deterministic mappings, we also introduce a time warping-invariant stochastic model referred to as *time warping-invariant stochastic QRNNs (TWI-SQRNNs)*.
- The capacity of TWI-QRNN and TWI-SQRNN model classes to successfully address time-warping transformations is exper-

imentally demonstrated on examples with classical or quantum dynamics.

2 Quantum Recurrent Neural Networks

Formally, we study the problem of mapping classical sequences $x_{1:T}$ comprising T samples x_t with $t = 1, 2, \dots, T$, to corresponding classical sequences $z_{1:T}$, comprising samples z_t with $t = 1, 2, \dots, T$, through a parameterized causal mapping operating over time t . The QRNN model in [22] implements a deterministic mapping between sequence $x_{1:T}$ and sequence $z_{1:T}$ based on a parameterized quantum circuit (PQC) for the case in which both x_t and z_t are real valued. We will specifically focus here on settings in which the target samples z_t are scalar, while input samples x_t may be arbitrary real vectors. In the following, we review the QRNN model, as well as the corresponding training criterion. Furthermore, we point out a connection between QRNNs and dissipative quantum neural networks (QNNs) [29][30], which will be leveraged in the following section to introduce the proposed model class.

2.1 Quantum Recurrent Neural Networks

A QRNN is defined by a parameterized unitary transformation $U(x, \theta)$ operating on a register of $n = n^A + n^B$ qubits. The unitary is a function of the real-valued input vector x and of a vector of real-valued model parameters θ . The ansatz, i.e., architecture, assumed in [22] for the unitary $U(x, \theta)$ includes an input encoding layer with single-qubit rotations dependent on input x , followed by parameterized processing layers with both single-qubit and two-qubit gates. Note, however, that we allow the dependence of the unitary $U(x, \theta)$ to be arbitrary. Therefore, the model accounts also for special input-encoding methods such as the repeat-until-success neural architecture from [21] (see also [31]).

As illustrated in Fig. 1, the unitary is applied at each time step by re-initializing the subregister of n^B qubits to the ground state $|0\rangle$. After the application of the unitary to all n qubits, the subregister of n^B qubits is measured. Since the subregister of n^A qubits is not measured, it can be used to propagate information from one time step to the next. Therefore, we will refer to the

n^A -qubit subregister as the *memory subregister*, while the subsystem of n^B qubits is referred to as the *output subregister*.

To elaborate, the density matrix describing the state of the register of n qubits before the first application of the unitary is given by $\rho_0^{AB} = |0\rangle\langle 0|^A \otimes |0\rangle\langle 0|^B$, where the first state is defined on the memory subregister of n^A qubits, and the second on the output subregister of n^B qubits as described by the superscripts A and B . Note that the memory subregister is also initialized to $|0\rangle$. The application of the unitary $U(x_1, \theta)$, which encodes the first input sample x_1 , yields the output state density $\rho_1^{AB} = U(x_1, \theta)\rho_0^{AB}U(x_1, \theta)^\dagger$. Then, a measurement is made on the output subregister.

The measurement is defined by a local observable O^B , which can always be expressed in a diagonal form $O^B = \sum_\lambda o_\lambda |\lambda\rangle\langle\lambda|^B$ in a suitable basis $|\lambda\rangle^B$. As a result of a measurement with outcome o_λ , the wavefunction of the output subregister collapses onto the state $|\lambda\rangle^B$; and the density matrix of the memory subregister is changed to the reduced density

$$\rho_1^{A|\lambda} = \frac{(I^A \otimes {}^B\langle\lambda|)\rho_1^{AB}(I^A \otimes |\lambda\rangle^B)}{{}^B\langle\lambda| \rho_1^B |\lambda\rangle^B}, \quad (1)$$

where we have $\rho_1^B = \text{Tr}_A(\rho_1^{AB})$ and $\text{Tr}_X(\cdot)$ indicates the partial trace with respect to subregister $X \in \{A, B\}$. In the QRNN model, the measurement is repeated many times in order to obtain an estimate of the expectation value $\langle O^B \rangle$ of the observable O^B . After averaging over the measurement outcomes, the resulting density matrix of the memory subregister is given by $\rho_1^A = \text{Tr}_B(\rho_1^{AB})$. Note that this description of the state of the memory subregister is independent of the specific observable O^B , and is sufficient to predict the expectations of downstream measurements [22]. Furthermore, we point the reader to Sec. 4, which studies a stochastic variant of the QRNN model in which a single measurement outcome o_λ is evaluated at each time step.

Generalizing to any time $t = 1, \dots, T$, the memory subregister evolves according to the update rules

$$\rho_t^{AB} = U(x_t, \theta)(\rho_{t-1}^A \otimes |0\rangle\langle 0|^B)U(x_t, \theta)^\dagger \quad (2)$$

and

$$\rho_t^A = \text{Tr}_B(\rho_t^{AB}), \quad (3)$$

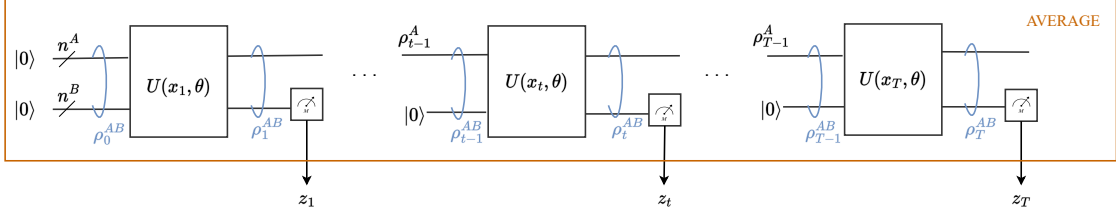


Figure 1: Illustration of the QRNN model introduced in [22].

with initialization $\rho_0^A = |0\rangle\langle 0|^A$. Furthermore, the output at each time t is given by a function

$$z_t = g(\langle O^B \rangle_t) \quad (4)$$

of the expected value

$$\langle O^B \rangle_t = \text{Tr}[\rho_t^{AB}(I^A \otimes O^B)] = \text{Tr}[\rho_t^B O^B] \quad (5)$$

of the local observable O^B , where $\rho_t^B = \text{Tr}_A[\rho_t^{AB}]$.

As mentioned earlier in this section and illustrated in Fig. 1, evaluating the sequence of expected values z_t requires running the circuit multiple times in order to approximately evaluate the expectations in (5) via empirical averages of the measurement outputs at all time steps $t = 1, \dots, T$.

2.2 Training QRNNs

Given a data set of input-output example pairs $(x_{1:T}, \bar{z}_{1:T})$, training of a QRNN targets the minimization of the training loss. To this end, for each example pair $(x_{1:T}, \bar{z}_{1:T})$, we define the quadratic training loss [22]

$$\ell(z_{1:T}, \bar{z}_{1:T}) = \frac{1}{T} \sum_{t=1}^T (\bar{z}_t - z_t)^2, \quad (6)$$

with z_t is a function of the model parameter vector θ through (4). The training loss (6) is averaged over all examples in the training set, and it can be minimized via zeroth-order optimization schemes, such as the parameter shift rule [32, 33].

2.3 QRNNs as Dissipative QNNs

In this subsection, we observe a useful connection between QRNNs and dissipative QNNs [29, 30], a popular model for PQCs that mimics the operation of classical multi-layer perceptrons. We specifically focus on single-layer QRNNs as defined in [29, Fig. 1]. A (single-layer) dissipative QNN encompasses an input subregister and

a number of output subregisters. A new output subregister is introduced at each processing step t , and a parameterized unitary U_t , also referred to as ‘‘perceptron’’, is applied to the input subregister and to the new output subregister. All output subregisters are finally measured. We note that dissipative QNNs are also related to quantum collision models used in quantum mechanics for the study of open quantum systems [34].

A dissipative QNN with $T = 3$ steps is illustrated in Fig. 2. Note that, unlike the dissipative QRNN model in [29, 30], in Fig. 2, a different input data sample x_t is loaded at each step t , and the unitaries $U(x_t, \theta)$ used across steps t share the same parameter vector θ . It can be readily checked that the dissipative QNN in Fig. 2 is equivalent to the QRNN model in Fig. 1 if we identify the input subregister of the dissipative QNN with the QRNN’s memory subregister and the output subregisters with the QRNN’s output subregister. This is in the sense that both models provide statistically equivalent outputs.

The main advantage of formulating a QRNN in terms of a dissipative QRNN is that the evolution of the system and the outputs given by (2)-(5) can be more directly expressed without explicitly resorting to partial trace operations and intermediate measurements at each time step t . To this end, define a system, as exemplified in Fig. 2 with $n_T = n_A + Tn_B$ qubits, corresponding to one memory subregister of n^A qubits and T output subregisters of n^B qubits. The output subregisters are indexed as $t = 1, 2, \dots, T$ as in Fig. 2. Initializing the density state of such system to the ground state $\rho_0 = |0\rangle\langle 0|$, where $|0\rangle$ is a separable ground state across the n_T qubits, the density state evolves as

$$\rho_{t+1} = V_t(x_t, \theta) \rho_t V_t(x_t, \theta)^\dagger, \quad (7)$$

where $V_t(x_t, \theta)$ is a unitary matrix that applies unitary $U(x_t, \theta)$ to the memory subregister (first wire in Fig. 2) and to the t -th output subregister,

while identity operators are applied to all other subregisters. Furthermore, the outputs (5) can be written as

$$\langle O^B \rangle_t = \text{Tr}[\rho_t O_t^B], \quad (8)$$

where the local observable O_t^B applies only to the t -th memory subregister.

3 Time Warping-Invariant QRNNs

In this section, we introduce the proposed TWI-QRNN model class. We start by defining the concept of time warping-invariance. Then, we derive the TWI-QRNN model, which is finally described, along with the corresponding training problem.

3.1 Time Warping-Invariance

Following [7] and [8], in order to define time warping-invariance, we consider a continuous-time formulation in which the time axis is defined by a real variable t . Round parentheses will be used to denote dependence on the continuous time t . Furthermore, we will take $a(t)$ to represent either the value of the function $a(\cdot)$ at time t , or the entire function $a(\cdot)$, as it will be clear from the context.

To start, we define a *time warping operation* $c(t)$ as any monotonically increasing function of time. Let us fix some subset \mathcal{C} of time warping operations. An example is given by the *linear time warping* family \mathcal{C} given by operations of the form $c(t) = at$ for some range of values $a > 0$, which correspond to a stretching ($a < 1$) or shrinking ($a > 1$) of the time axis. Time warping-invariance is a property of a parameterized model class $z(t) = f(x(t), \theta)$ of mappings between an input continuous-time signal $x(t)$ and an output continuous-time signal $z(t)$. Note that the mapping is arbitrary, and not restricted to memoryless functions. Furthermore, a mapping in the class is identified by the model parameter θ .

Model class $f(\cdot, \theta)$ is said to be *time warping-invariant* with respect to the family \mathcal{C} , if for any $z(t) = f(x(t), \theta)$ produced by the model with some model parameters θ given input $x(t)$, there exist model parameters θ' that yield the output $z(c(t)) = f(x(c(t)), \theta')$ given input $x(c(t))$ for any function $c(t)$ in \mathcal{C} . In words, the model class

can reproduce time-warped versions of its input-output pairs.

It is emphasized that the definition of time warping-invariance given above applies only to continuous-time processes. Therefore, its extension to discrete-time processes, first introduced in [7], requires the use of discrete-time approximations. As we detail in the next subsection, these approximations entail that the notion of time warping-invariance is more loosely defined as compared to the “spatial” invariances studied in quantum geometric machine learning [13]. We may hence refer to the resulting invariance property as a *quasi*-invariance as in [7], but we will not make this distinction explicit in the following.

3.2 Time Warping-Invariance for QRNNs

The time warping-invariance property defined in the previous subsection can be applied to QRNNs as long as one specifies a suitable continuous-time extension of the defining equalities (2)-(5), or equivalently (7)-(8). Here, we adopt a stronger definition of time warping-invariance based on the formulation (7)-(8), whereby the invariance condition is imposed on the input-output pairs (x_t, ρ_t) . Note that, if invariance holds in terms of the density matrices ρ_t , then it also holds, a fortiori, on the expected values (8) producing the output samples z_t . In the rest of this subsection, we provide a derivation of the TWI-QRNN model that differs from the steps of classical models [7], [8] and is more suitable for a quantum mechanical description of the problem. A direct extension of the arguments in [7], [8] can be found in the Appendix. The reader only interested in the definition of the model can move on directly to the next subsection.

Let us start from the definition (7) and apply a time-warping operation so that the input signal observed by the QRNN at time t is given by $x(c(t))$. Denote as $\rho(t)$ a continuous-time version of the density matrix ρ_t obtained with the original input $x(t)$, and as $\rho(c(t))$ the corresponding density matrix obtained with the time-warped input $x(c(t))$ under time warping-invariance. The change in density matrix from one discrete-time step t to the next, $t + 1$, can be related to the derivatives with respect to the warped time axis as

$$\rho(c(t+1)) - \rho(c(t)) = \int_t^{t+1} \frac{d\rho(c(t))}{dc(t)} \frac{dc(t)}{dt} dt, \quad (9)$$

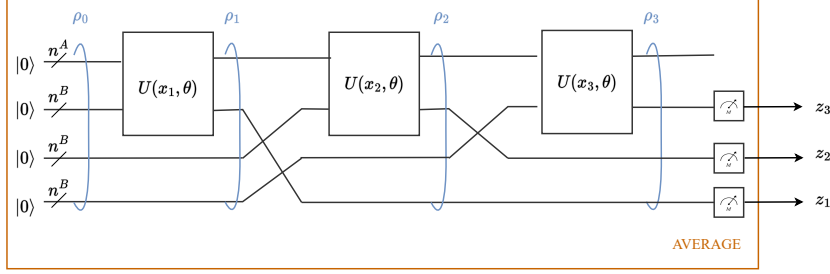


Figure 2: The QRNN model in Fig. 1 can be interpreted as a variant of a dissipative QRNN [29, 30], as shown in the figure with $T = 3$, in which the same parameter vector θ is reused by unitaries $U(x, \theta)$, and different data samples x_t are loaded at each time t .

where we have used the definition of integral and changed the integration variable from $c(t)$ to t .

To proceed, we make the approximation of considering the time-warping derivative $dc(t)/dt$ to be constant in the interval $[t, t+1]$, so that it can be taken out of the integral in (9). Furthermore, in order to account for the desired time warping-invariance of the output density matrix, we assume that the continuous-time evolution operator is approximately invariant under time-warping transformations, i.e.,

$$\frac{d\rho(c(t))}{dc(t)} \approx \frac{d\rho(t)}{dt}. \quad (10)$$

With regards to the approximations put forth in this paragraph, we note that we are only interested in the evolution of the density at the end of the discrete time-step from time t to $t+1$ as per (7), and hence we can ignore constraints on the underlying infinitesimal physical evolution as long as they are consistent with the discrete-time evolution. Importantly, we emphasize that the approximate equality (10) is not intended to indicate that a meaningful continuous-time physical process $\rho(t)$ exists that satisfies (10) with a strict equality. Rather, the continuous-time quantum process is just used as a motivational starting point for the introduction of the TWI-QRNN model. For clarity, and to acknowledge the approximations made, we will use $\tilde{\rho}(\cdot)$ in the rest of the derivation.

Inserting (10) into (9) and using the above approximations, we obtain

$$\begin{aligned} \tilde{\rho}(c(t+1)) - \tilde{\rho}(c(t)) &\approx \frac{dc(t)}{dt} \int_t^{t+1} \frac{d\tilde{\rho}(t)}{dt} dt \\ &= \frac{dc(t)}{dt} (\tilde{\rho}(t+1) - \tilde{\rho}(t)). \end{aligned} \quad (11)$$

In (11), the density $\tilde{\rho}(t+1)$ is given by the output of the QRNN, via (7), with previous state $\tilde{\rho}(c(t)) \approx \tilde{\rho}(t)$. Moreover, from the point of view of a discrete QRNN model under time warping, the time $c(t)$ corresponds to discrete time t , the value $x(c(t))$ to sample x_t , and density matrix $\tilde{\rho}(c(t))$ to $\tilde{\rho}_t$. Using these definitions, we get the approximate equality

$$\tilde{\rho}_{t+1} \approx \left(1 - \frac{dc(t)}{dt}\right) \tilde{\rho}_t + \frac{dc(t)}{dt} V_t(x_t, \theta) \tilde{\rho}_t V_t(x_t, \theta)^\dagger. \quad (12)$$

We observe that the right-hand side in (12) is a valid density matrix if the inequality $dc(t)/dt \leq 1$ holds. The same limitation applies to the derivation presented in [7] for classical models (see also Appendix), and it stems from approximations done in going from discrete to continuous time and back.

In other words, under condition (12), the density matrix $\tilde{\rho}_{t+1}$ is produced by leaving the previous density matrix $\tilde{\rho}_t$ unchanged with probability $(1 - dc(t)/dt)$ and by applying the unitary $V_t(x_t, \theta)$ otherwise. The update (12) is the key equation defining TWI-QRNNs, as it will be elaborated on in the next subsection.

3.3 TWI-QRNNs

Based on the analysis in the previous subsection, we define the class of TWI-QRNNs using the partial trace formalism (2)-(5) as follows. A TWI-QRNNs applies the updates

$$\begin{aligned} \rho_t^{AB} &= (1 - \alpha_t)(\rho_{t-1}^A \otimes |0\rangle\langle 0|^B) \\ &+ \alpha_t U(x_t, \theta)(\rho_{t-1}^A \otimes |0\rangle\langle 0|^B)U(x_t, \theta)^\dagger, \end{aligned} \quad (13)$$

where $\alpha_t \in [0, 1]$ is a probability, along with the equalities (3)-(5). Accordingly, when evaluating

the output z_t for time t , a TWI-QRNN generates a number of realizations of $t-1$ Bernoulli random variables b_1, \dots, b_{t-1} , with each random variable $b_t \sim \text{Bern}(\alpha_t)$ being equal to 1 with probability α_t . For each realization b_1, \dots, b_{t-1} , at time $t' < t$, a unitary $U(x_{t'}, \theta)$ is applied to the memory and output subregisters if $b_{t'} = 1$ and an identity is applied otherwise, followed by a measurement of the output register. The outputs of the measurement of the output register at time t are then averaged to obtain z_t .

By the analysis in the previous subsection, culminating in (12), the probability α_t should be chosen equal to the time-warping derivative $dc(t)/dt$. To gain insight on this selection, let us consider the case of a linear time warping family \mathcal{C} defined as $c(t) = at$ with $a < 1$, which corresponds to a stretching the inputs and outputs by a factor of $1/a$. Accordingly, by the definition of time warping-invariance, if the input x_t is stretched by a factor of $1/a$, the model class should be able to reproduce an equally stretched density output sequence ρ_t . Therefore, assuming $1/a$ to be an integer, if each input sample x_t of the original sequence is kept constant for $1/a$ consecutive samples, the output samples ρ_t of the output sequence should also be constant for consecutive intervals of $1/a$ samples. The update (13) implements a probabilistic version of this operation, whereby each sample ρ_t is held constant, on average, for $1/(1 - \alpha_t)$ consecutive samples. Therefore, setting $\alpha_t = 1 - a$ approximately satisfies time warping-invariance with respect to the family \mathcal{C} .

We finally observe that the mechanism described in this subsection, which is based on $t-1$ classical binary variables and switches, could be readily replaced by a fully quantum implementation with controlled- U gates and $t-1$ of controlling ancilla qubits. However, this alternative architecture is rather inefficient for sequences containing a sufficiently large number of time samples.

3.4 Adaptive Gating Mechanism

Whilst the motivational derivation above suggests the choice of α as $dc(t)/dt$, the proposed algorithm practically replaces the unknown derivative in the model (13) with a classical recurrent neural network model (RNNs) that infers a suitable time-warping probability α_t from the input

data sequence in a causal fashion. Specifically, we write the probability α_t as

$$\alpha_t = \sigma(\phi_t), \quad (14)$$

where $\sigma(a) = (1 + \exp(-a))^{-1}$ denotes a logistic sigmoid with *hyperparameter vector* ϕ_t being the output of a model defined by the updates

$$\phi_t = W_x x_t + W_h h_t + b, \quad (15)$$

and

$$h_t = \tanh(W_x^h x_t + W_h^h h_{t-1} + b), \quad (16)$$

where $W = \{W_x, W_h, W_x^h, W_h^h\}$ denote learnable parameters. The overall TWI-QRNN model is shown in Fig. 3.

We emphasize that the classical RNN model is not required if one has prior knowledge of the time-warping function. Furthermore, we intentionally avoid introducing gating mechanisms in the RNN. This choice is motivated by the designated role of the RNN as a mechanism to estimate the time-warping function, with the model memory being managed by the quantum system via the described gating scheme. That said, we note that more complex tasks may call for more sophisticated gating mechanisms across both quantum and classical models.

3.5 Training TWI-QRNNs

Let us define as

$$q(b_t | x_{1:t}, W) = \sigma(\phi_t)^{b_t} (1 - \sigma(\phi_t))^{1-b_t} \quad (17)$$

the variational distribution of the Bernoulli variable b_t dictating whether or not the current unitary $U(x_t, \theta)$ is applied to the input and memory subregisters as per (13). The joint distribution of the variables $b_{1:T}$ is then given as $q(b_{1:T} | x_{1:T}, W) = \prod_{t=1}^T q(b_t | x_{1:t}, W)$. Note that the samples $b_{1:T}$ are conditionally independent given the input sequence $x_{1:T}$, and that the variable b_t depends causally on the input samples $x_{1:T}$. Training a TWI-QRNN amounts to the optimization of the variational parameters W and of the PQC parameters θ .

To specify the training problem, we define the loss for each example $(x_{1:T}, \bar{z}_{1:T})$ as the expectation $\mathbb{E}[\ell(z_{1:T}, \bar{z}_{1:T})]$ of the loss function (6), where the average is taken with respect to the random

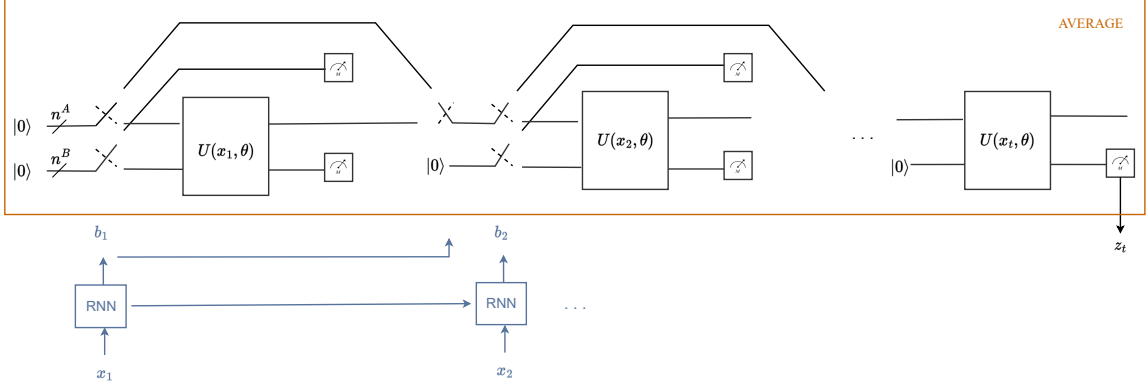


Figure 3: Illustration of the operation of the TWI-QRNN model.

variables $b_{1:T}$, which, in turn, determine the random outputs $z_{1:T}$. To estimate this expectation, one can leverage realizations of the outputs $z_{1:T}$ obtained as described in the previous subsection by drawing samples from the variational distribution $q(b_{1:T}|x_{1:T}, W)$.

The resulting training loss is minimized via gradient descent over W . Specifically, the variational parameters W are optimized using the log-derivative trick [35] to estimate the gradient, whilst optimization over θ is carried out using zeroth-order optimization as for QRNNs.

4 Stochastic Time Warping-Invariant QRNNs

In this section, we introduce a probabilistic counterpart of the QRNN, referred to as stochastic QRNN (SQRNN), which is then extended to the time warping-invariant class TWI-SQRNN.

4.1 SQRNNs

A SQRNN is a probabilistic model that maps an input real-valued vector sequence $x_{1:T}$ to a discrete-valued sequence $y_{1:T}$, with y_t being a string of n_B bits. Note that equivalently, we can consider the output sample y_t to take one out of 2^{n_B} possible values. Accordingly, without loss of generality, we write $y_t \in \{0 : 2^{n_B} - 1\}$. Unlike the QRNN model introduced in Sec. II, an SQRNN outputs sequence $y_{1:T}$ via a *single* run of the circuit, hence not requiring an empirical average over multiple runs of the circuit. Specifically, as illustrated in Fig. 4, the output y_t is the random output of the measurement of the output subregister at time t .

To elaborate, let us fix a projective measure-

ment defined by projection matrices Π_y^B with $y \in \{0 : 2^{n_B} - 1\}$. The projection matrices act on the output subregister. Then, the probability of the outcome y_t at time t given the past and current samples $x_{1:t}$ of the input sequence is given by Born's rule as

$$p(y_t | x_{1:t}, \theta) = \text{Tr}(\rho_t^{AB} (I^A \otimes \Pi_{y_t}^B)), \quad (18)$$

where Π_{y_t} is applied only to the output subregister and the density matrix ρ_t^{AB} is defined as in Sec. 2.

Given an example $(x_{1:T}, \bar{y}_{1:T})$, the training loss is defined as the cross-entropy loss

$$\begin{aligned} \ell(x_{1:T}, \bar{y}_{1:T}) &= -\frac{1}{T} \sum_{t=1}^T \log p(\bar{y}_t | x_{1:t}, \theta) \\ &= -\frac{1}{T} \sum_{t=1}^T \log \text{Tr}(\rho_t^{AB} (I^A \otimes \Pi_{\bar{y}_t}^B)). \end{aligned} \quad (19)$$

We observe that this loss is the negative logarithm of the product of conditional marginals. Its minimization may be interpreted as a form of pseudo maximum likelihood [36]. An alternative, but more complex, criterion would be the negative logarithm of the joint distribution of sequence $\bar{y}_{1:T}$, which can be obtained from the joint density ρ_t described in Sec. 2.3. The training problem with loss (19) can be addressed using the same tools mentioned in Sec. 2 for QRNNs.

4.2 TWI-SQRNNs

In the previous section, we have introduced TWI-QRNNs by imposing time warping-invariance in terms of the density matrices produced by the equivalent dissipative QNN. Since the probabilities (18) have the same form as the expectations

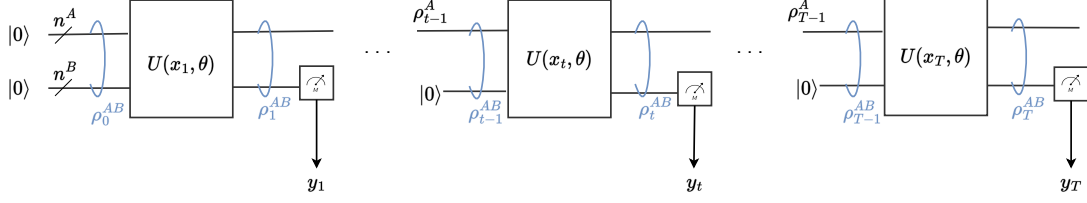


Figure 4: Illustration of the proposed SQRNN model.

(5) defining the outputs of QRNNs, the same reasoning applies to SQRNNs ρ_t^{AB} .

Based on this observation, we define TWI-SQRNNs in a manner analogous to TWI-QRNNs. The only caveat is that each output y_t is obtained via a *single* pass through the circuit up to time t , rather than by carrying out several runs through the circuit. Accordingly, when evaluating the output y_t for time t , a TWI-SQRNN generates a single realization of $t - 1$ Bernoulli random variables b_1, \dots, b_{t-1} , with each random variable $b_t \sim \text{Bern}(\alpha_t)$ being equal to 1 with probability α_t in (14). For the given realization b_1, \dots, b_{t-1} , at time $t' < t$, a unitary $U(x_{t'}, \theta)$ is applied to the memory and output subregisters if $b_{t'} = 1$ and an identity is applied otherwise, followed by a measurement of the output register.

Finally, training is carried out in a manner analogous to TWI-QRNNs by defining the training loss as the expectation of the cross-entropy loss (19) with respect to the variational distribution $q(b_{1:T}|x_{1:T}, W)$.

5 Experiments

In this section, we provide experimental results to elaborate on the performance of TWI-QRNNs – and their stochastic counterpart, TWI-SQRNNs – as opposed to conventional (s)QRNNs, in the presence of time-warping distortions of the input sequence.

5.1 Learning Tasks

5.1.1 Remembering a Cosine Wave

To start, we consider the task of remembering the past sample of a simple classical time sequence x_t , namely a, possibly time-warped, discrete-time cosine function. Accordingly, we set the target sequence as $\bar{z}_t = x_{t-1}$ for (TWI-)QRNNs and $y_t = x_{t-1}$ for (TWI-)SQRNNs. For the case without time warping, reference [22] demonstrated

that the original QRNN model is capable of successfully implementing this task. In contrast, here we study the robustness of the models under study to a time warping of the input sequence. To elaborate, the considered cosine function is given by

$$\cos(t) = \frac{\cos(\pi \frac{t}{5}) + 1}{2}. \quad (20)$$

The “unwarped” sequence in (20) is shown in Fig. 5(left) for $T = 200$ samples $x_t = \cos(t)$ obtained at time instants $t = 1, 2, \dots, T$, $T = 200$. For the stochastic models, which produces discrete outputs, the value of the cosine in (20) is discretized to 2^{n_B} levels equally spaced in the interval $[-1, 1]$ with $n_B = 3$ (see next subsection for further details on the model architecture).

We apply linear time-warping to obtain “warped” input sequences x_t as discussed in Sec. 3.3. Accordingly, given the unwarped sequence x_t obtained by sampling the original cosine signal $\cos(t)$, we repeat each sample for $1/a$ time instants, where a is such that the ratio $1/a$ is an integer. This setting accounts for a sampler with memory, as a new sample is observed every $1/a$ time steps. Examples of warped sequences x_t are shown in Fig. 5 for $a = 0.1$ (middle) and $a = 0.05$ (right).

5.1.2 Predicting Spin Dynamics

Following [22], we study next the problem of predicting the expected value of an observable for the quantum spin dynamics of a three-qubit system. The density state $\sigma(t)$ of the three-qubit system evolves in continuous time according to the Lindblad master equation

$$\begin{aligned} \frac{d\sigma(t)}{dt} = & -i[H, \sigma(t)] \\ & + \frac{1}{2} \sum_i \left[2C_k \sigma(t) C_k^\dagger - \sigma(t) C_k^\dagger C_k - C_k^\dagger C_k \sigma(t) \right], \end{aligned} \quad (21)$$

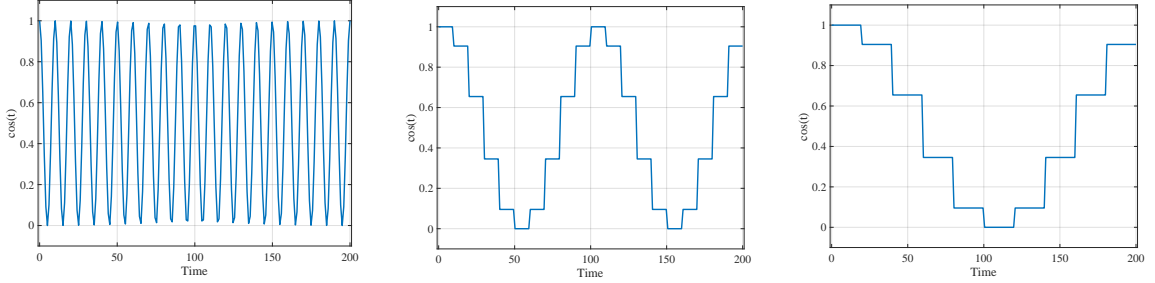


Figure 5: (left) The “unwarped” cosine function (20) used for the first experiment (as in [22]); and the corresponding (linearly) time-warped signals for $a = 0.1$ (middle) and $a = 0.05$ (right).

with Hamiltonian

$$H = -\frac{1}{2} \sum_{i=1}^3 h_i Z_i - \frac{1}{2} \sum_{i=1}^2 (J_i X_i X_{i+1} + J_i Y_i Y_{i+1} + J_i Z_i Z_{i+1}), \quad (22)$$

and matrices $C_k = c(X_k + Y_k)$. The coefficients are set to $h_k = 2\pi$, $J_k = 0.1\pi$, and the dissipation rate equals $c = \sqrt{0.0002}$. The initial state is set to $\rho(0) = |+\rangle^{\otimes n}$, and the sequence is sampled at continuous time instants $\Delta T, 2\Delta T, \dots, 200\Delta T$ with $\Delta T = 1/20$, which correspond to the discrete time instants $t = 1, 2, \dots, T$, respectively, with $T = 200$. The unwarped input x_t is then given by the corresponding expected values of the Z observable for the first qubit of the three qubits.

Non-linear time-warped sequences are generated by setting $c(t) = \sqrt{t}$, and sampling the solution of the master equation (22) at continuous time instants $\sqrt{\Delta T}, \sqrt{2\Delta T}, \dots, \sqrt{200\Delta T}$, which correspond to the discrete time instants $t = 1, 2, \dots, T = 200$. This setting represents an instance in which the sampling interval varies over time.

5.2 Architectures and Hyperparameters

5.2.1 Circuit

Throughout this section, we adopt models with $n = 6$ qubits consisting of an $n_A = 3$ -qubit memory subregister and of an $n_B = 3$ -qubit output subregister. The parameterized unitary $U(x, \theta)$ implements the cascade of an *encoding unitary* $U_{in}(x)$, and of a problem-dependent *evolution unitary* $U_H(\theta)$. Specifically, in order to encode

each input sample x we use the encoding unitary $U_{in}(x) = I^A \otimes R_{in}(x)^{\otimes 3}$, which applies an identity transformation to the memory subregister and an input-dependent Pauli- Y rotation [22]

$$R_{in}(x) = R_y(\arccos(x)) = \exp(-i\arccos(x)Y/2) \quad (23)$$

to each qubit of the output register. As shown in Fig. 7, the evolution unitary consists of a layer of single qubit rotation gates, each parameterized by the angles θ as in [22], followed by Hamiltonian dynamics. Thereby, after the rotation layer, the unitary transformation $\exp(-iH\Delta t)$ is applied using the fixed Hamiltonian

$$H = \sum_{i=1}^n a_i X_i + \sum_{i=1}^n \sum_{j=1}^{i-1} J_{ij} Z_i Z_j \quad (24)$$

with $\Delta t = 0.17$. The coefficients a_i, J_{ij} in (24) are drawn randomly from a uniform distribution as $a_i, J_{ij} \in [-1, 1]$, and they are fixed during training. In contrast, the rotation angles are optimized using the gradient-free optimizer COBLYA [37]. We emphasize that the encoding circuit could be chosen differently, and that the architecture has not been optimized. For example, we may be able to improve the performance of the models by encoding orthogonal polynomials or using trainable encoding strategies [38]. At the measurement part, we measure Z-expectation value of each qubit in the output register and take z_t as their average multiplied by a real coefficient c for the (TWI)-QRNN.

5.2.2 Gating Mechanism via a Classical RNN

For the classical RNN in the proposed models, we do not use hidden layers and we directly optimize

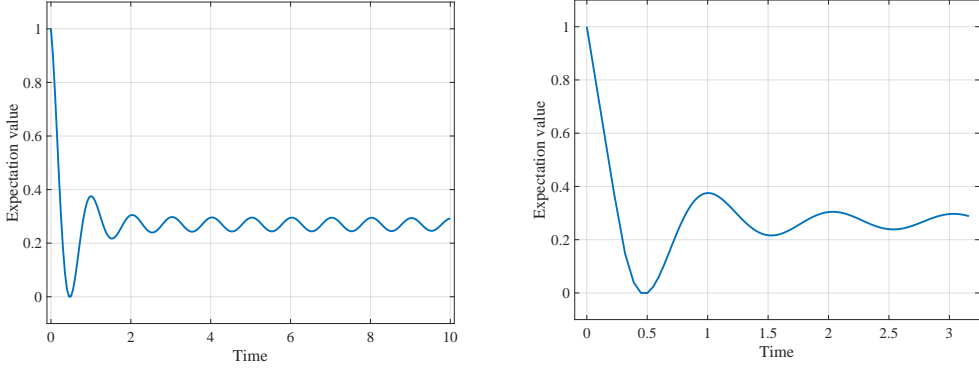


Figure 6: (left) The “unwarped” expected value of the observable for the three-qubit spin dynamics generated by (21); and (right) the corresponding time-warped signal with non-linear transformation $c(t) = \sqrt{t}$.

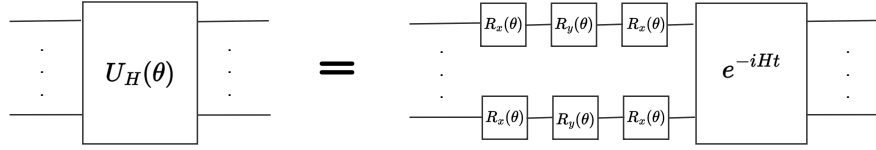


Figure 7: The evolution part of the circuit utilized in the numerical simulations. The rotation angles θ act as parameters of the circuit. The Hamiltonian H is fixed and given by (24).

the gating parameters $W = \{W_x, W_h, W_x^h, W_h^h\}$ determining the hyperparameter in (15) using gradient descent as discussed in Sec. III-D. The optimization of the circuit and gating parameters is carried over in an iterative manner.

5.3 Results

5.3.1 Remembering a Cosine Wave

For the first task – remembering the last sample of a, possibly time-warped, cosine wave – we show the accumulated prediction loss over time in Fig. 8. The training algorithm is run for the first 50 samples (not shown), and the error is accumulated over the subsequent 150 samples. We use 5 trials, and we average over the random initialization of the trainable parameters, as well as the Hamiltonian coefficients in (24).

We consider the case when the warping parameter a is known a priori, as well as the more challenging case in which parameter a is not known and is learnt via the proposed RNN-based adaptive gating mechanism. For both considered value of a , namely $a = 0.1$ and $a = 0.05$, the proposed TWI-QRNN model is seen to consistently achieve a significantly lower loss as compared with the standard QRNN. This demonstrates the robust-

ness of TWI-QRNNs to linear time warps. The gap in performance between TWI-QRNNs and QRNNs widens as time warping becomes more pronounced by having a increase from $a = 0.1$ to $a = 0.05$. Similar conclusions can be drawn for the stochastic model, as shown in Fig. 9. In fact, TWI-SQRNN outperforms the SQRNN model for both values of a .

Overall, for both models, the gating mechanism is seen to be capable of adapting the value of a , achieving comparable loss to the case when a is known a priori. In fact, the loss obtained with adaptive gating is lower than that with known parameter a . This suggests that the adaptive gating mechanism, which is further investigated in Appendix A, may compensate for errors in the approximations adopted in Sec. 3.

5.3.2 Predicting Spin Dynamics

In a manner similar to the previous experiment, the accumulated quadratic loss for the problem of predicting spin dynamics over time is shown in Fig. 10. We consider again both the ideal case in which the time-warping function $c(t) = \sqrt{t}$ is known a priori, and the more practical case in which the time transformation is not known

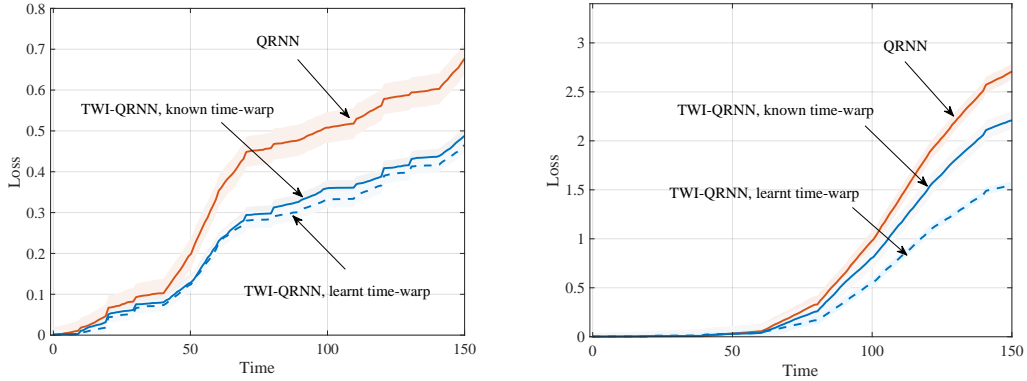


Figure 8: Cumulative quadratic loss for the task of remembering a time-warped cosine wave as a function of time for time-warping parameters $a = 0.1$ (left) and $a = 0.05$ (right).

and is learnt via the RNN-based adaptive gating mechanism.

The accrued loss accumulates more quickly in the earlier time steps as the warping is more prominent when the continuous time variable t is smaller. However, the proposed model is seen to be capable of resisting even non-linear warping transformations, accruing much lower prediction loss over time compared to the conventional QRNN model. This confirms that the gating mechanism can approximate the warping derivative and achieve low prediction loss, encouraging the use of the proposed model for prediction of phenomena characterized by quantum dynamics.

6 Discussion and Future Work

In this paper, we have studied quantum models that process temporal data. We have showed that postulating invariance to time transformations in the data, hence taking invariance to time warping as an axiom, necessarily leads to an adaptive gate-like mechanism in quantum recurrent models. We derived a novel quantum model class from first principles, which was experimentally seen to be capable of resisting time warping transformations.

Various future research directions arise. For example, it is an open question how to design an efficient TWI-QRNN models with a fully quantum gating mechanism. This is particularly useful for running the models on quantum hardware, rather than simulators, and it is also left for future work. Finally, it is important to identify instances in which the proposed model class

may offer improvements as compared to classical gated architectures, such as the gated LSTM model. An interesting direction could be the investigation of the memory cost of time warping-invariant quantum recurrent models, since quantum models have been shown to describe temporal sequences with reduced memory [25, 24]. Given the performance of the proposed model on prediction tasks, we expect it to be advantageous for tasks related to quantum phenomena, with extensions possibly operating directly on quantum data [39].

Acknowledgements

We would like to thank Johannes Bausch and Danilo Rezende for reviewing the paper prior to submission. OS acknowledges funding from the European Research Council (ERC) under the European Union’s Horizon 2020 Research and Innovation Program (Grant Agreement No. 725731) and from the EPSRC (EP/W024101/1). LB acknowledges funding from the U.S. Department of Energy, Office of Science, National Quantum Information Science Research Centers, Superconducting Quantum Materials and Systems Center (Contract No. DE-AC02-07CH11359).

A Further Experiments

In this appendix, we provide further insights on the extent to which the trained RNN fits the time-warping derivative $dc(t)/dt$. As demonstrated in Sec. 5 via experiments, the choice $\alpha_t \approx dc(t)/dt$, which is motivated by the heuristic derivation of

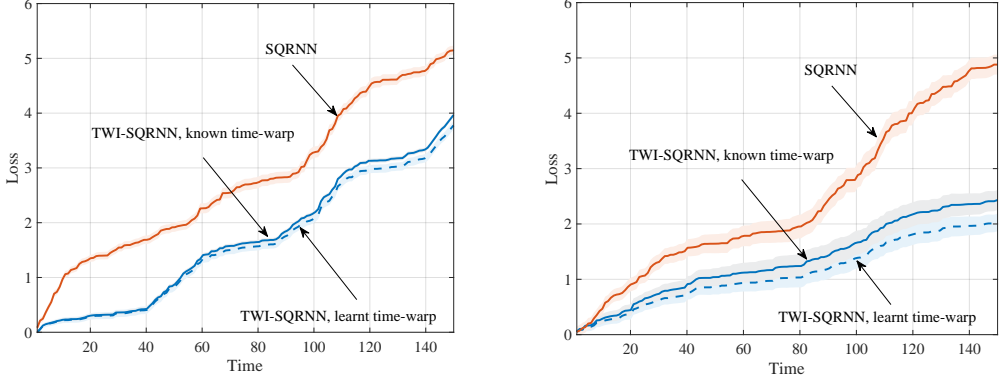


Figure 9: Cumulative quadratic loss for the task of remembering a time-warped cosine wave as a function of time for time-warping parameters $a = 0.1$ (left) and $a = 0.05$ (right). Unlike Fig. 8, which considers deterministic predictors obtained via expected values of an observable, this figure consider stochastic, one-shot, predictors based on a single measurement output (see Sec. 4).

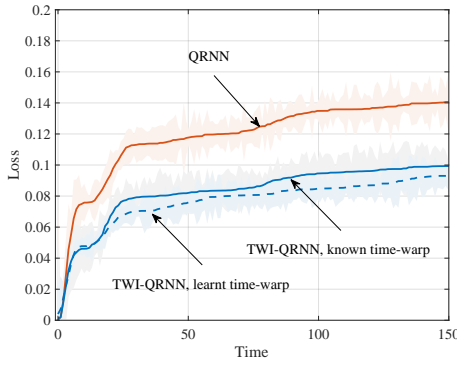


Figure 10: Cumulative quadratic loss for the task of predicting time-warped spin dynamics as a function of time for time-warping function $c(t) = \sqrt{t}$.

the TWI-QRNN model in Sec. 3.2, is generally suboptimal in terms of performance loss. In fact, as seen in Fig. 8 and Fig. 9, the performance obtained with the ‘known’ time-warp $\alpha_t \approx dc(t)/dt$ is improved by the ‘learnt’ time-warp α_t in (14) obtained via the RNN.

To this end, Fig. 11 illustrates the known time-warping derivative $dc(t)/dt$ and learnt time-warping derivatives α_t in (14) for the two examples studied in Sec. 5, which involve linear and non-linear warping. Whilst the output α_t of the RNN is seen to approximate the derivative $dc(t)/dt$, in both cases the match is not perfect. Together with the observations made in Fig. 8 and Fig. 9, this confirms that setting $\alpha = dc(t)/dt$ is generally not optimal, and the RNN may effectively compensate for the some of the approximation errors introduced in deriving the model in (10).

B Alternative Derivation of TWI-QRNNs

In this section, we present an alternative derivation of the TWI-QRNN model that follows directly the steps in [7]. To start, we introduce a continuous-time version of the update (7) via the approximation

$$\rho(t + \delta t) \approx \rho(t) + \frac{d\rho(t)}{dt} \delta t, \quad (25)$$

where we have used $\rho(t)$ to denote a continuous-time version of the density matrix and $\delta t > 0$ is a time interval. The update (7) can be viewed as the standard *Euler approximation* of (25). Accordingly, under suitable assumptions, the accuracy of the approximation is proportional to δt (see, e.g., [40, Chapter 4]). It is emphasized that (25) is not meant to be a description of the continuous-time dynamics of the system, which is dictated by the Liouville–von Neumann equation [41], but only a stepping stone in the derivation of time warping-invariant discrete-time models.

From (7), setting $\delta t = 1$, we then have

$$\frac{d\rho(t)}{dt} = V(x(t), \theta)\rho(t)V(x(t), \theta)^\dagger - \rho(t), \quad (26)$$

where we have kept the dependence of the unitary $V(x(t), \theta)$ on time t implicit. Let us now apply a time-warping operation so that the input signal observed by the QRNN at time t is given by $x(c(t))$. Using (26), the output density satisfies

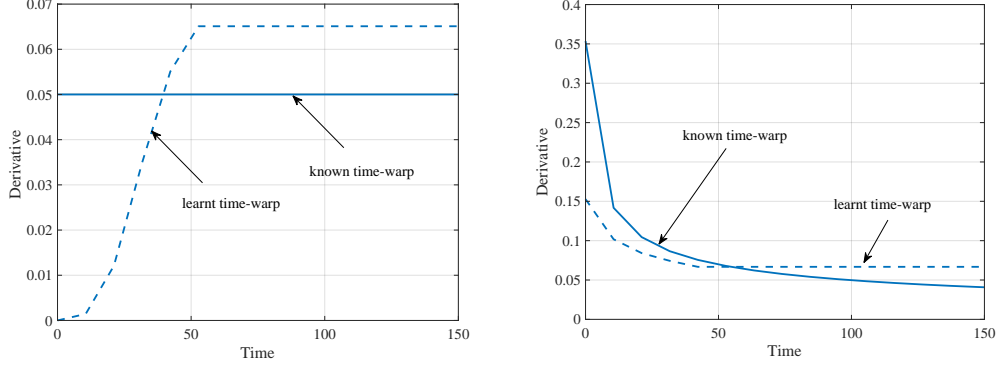


Figure 11: (left) Known time-warping derivative $dc(t)/dt$ and learnt derivative α_t in (14) for linear warping $c(t) = at$; and (right) for non-linear warping $c(t) = \sqrt{t}$.

the equality

$$\begin{aligned} \frac{d\rho(c(t))}{dc(t)} &= V(x(c(t)), \theta)\rho(c(t))V(x(c(t)), \theta)^\dagger \\ &\quad - \rho(c(t)). \end{aligned} \quad (27)$$

Using the chain rule of differentiation, this in turn yields

$$\begin{aligned} \frac{d\rho(c(t))}{dt} &= \frac{d\rho(c(t))}{dc(t)} \cdot \frac{dc(t)}{dt} \\ &= \frac{dc(t)}{dt} [V(x(c(t)), \theta)\rho(c(t))V(x(c(t)), \theta)^\dagger \\ &\quad - \rho(c(t))]. \end{aligned} \quad (28)$$

To obtain a relationship between density matrices $\rho(c(t+1))$ and $\rho(c(t))$, we take a Taylor expansion on the time-warped model, whereby we obtain

$$\rho(c(t + \delta t)) \approx \rho(c(t)) + \frac{d\rho(c(t))}{dt} \delta t. \quad (29)$$

By plugging in (28), and taking $\delta t = 1$, this yields

$$\begin{aligned} \rho(c(t + 1)) &= \left(1 - \frac{dc(t)}{dt}\right) \rho(c(t)) \\ &\quad + \frac{dc(t)}{dt} V(x(c(t)), \theta)\rho(c(t))V(x(c(t)), \theta)^\dagger. \end{aligned} \quad (30)$$

Following the arguments in [7] and [8], we finally return to a discrete-time model as follows. From the point of view of a discrete QRNN model under time warping, the time $c(t)$ corresponds to discrete time t , the value $x(c(t))$ to x_t , and $\rho(c(t))$ to ρ_t . Therefore, a discrete-time version of (30) can be defined as (12).

References

- [1] K. Chowdhary, “Natural language processing,” *Fundamentals of artificial intelligence*, pp. 603–649, 2020.
- [2] J. Hirschberg and C. D. Manning, “Advances in natural language processing,” *Science*, vol. 349, no. 6245, pp. 261–266, 2015.
- [3] I. M. Georgescu, S. Ashhab, and F. Nori, “Quantum simulation,” *Reviews of Modern Physics*, vol. 86, no. 1, p. 153, 2014.
- [4] K. Mitarai, M. Negoro, M. Kitagawa, and K. Fujii, “Quantum circuit learning,” *Physical Review A*, vol. 98, no. 3, p. 032309, 2018.
- [5] A. Graves, “Long short-term memory,” *Supervised sequence labelling with recurrent neural networks*, pp. 37–45, 2012.
- [6] A. Graves, A.-r. Mohamed, and G. Hinton, “Speech recognition with deep recurrent neural networks,” in *2013 IEEE international conference on acoustics, speech and signal processing*. Ieee, 2013, pp. 6645–6649.
- [7] C. Tallec and Y. Ollivier, “Can recurrent neural networks warp time?” *arXiv preprint arXiv:1804.11188*, 2018.
- [8] M. M. Bronstein, J. Bruna, T. Cohen, and P. Veličković, “Geometric deep learning: Grids, groups, graphs, geodesics, and gauges,” *arXiv preprint arXiv:2104.13478*, 2021.
- [9] P. Veličković, G. Cucurull, A. Casanova, A. Romero, P. Lio, and Y. Bengio, “Graph attention networks,” *arXiv preprint arXiv:1710.10903*, 2017.

[10] A. Krizhevsky, I. Sutskever, and G. E. Hinton, “Imagenet classification with deep convolutional neural networks,” *Advances in neural information processing systems*, vol. 25, pp. 1097–1105, December, 2012.

[11] M. Larocca, F. Sauvage, F. M. Sbahi, G. Verdon, P. J. Coles, and M. Cerezo, “Group-invariant quantum machine learning,” *arXiv preprint arXiv:2205.02261*, 2022.

[12] J. J. Meyer, M. Mularski, E. Gil-Fuster, A. A. Mele, F. Arzani, A. Wilms, and J. Eisert, “Exploiting symmetry in variational quantum machine learning,” *arXiv preprint arXiv:2205.06217*, 2022.

[13] M. Ragone, P. Braccia, Q. T. Nguyen, L. Schatzki, P. J. Coles, F. Sauvage, M. Larocca, and M. Cerezo, “Representation theory for geometric quantum machine learning,” *arXiv preprint arXiv:2210.07980*, 2022.

[14] G. Verdon, M. Broughton, J. R. McClean, K. J. Sung, R. Babbush, Z. Jiang, H. Neven, and M. Mohseni, “Learning to learn with quantum neural networks via classical neural networks,” *arXiv preprint arXiv:1907.05415*, 2019.

[15] G. Verdon, T. McCourt, E. Luzhnic, V. Singh, S. Leichenauer, and J. Hidary, “Quantum graph neural networks,” *arXiv preprint arXiv:1909.12264*, 2019.

[16] X. Ai, Z. Zhang, L. Sun, J. Yan, and E. Hancock, “Decompositional quantum graph neural network,” *arXiv preprint arXiv:2201.05158*, 2022.

[17] P. Mernyei, K. Meichanetzidis, and I. I. Ceylan, “Equivariant quantum graph circuits,” in *International Conference on Machine Learning*. PMLR, 2022, pp. 15 401–15 420.

[18] Q. T. Nguyen, L. Schatzki, P. Braccia, M. Ragone, P. J. Coles, F. Sauvage, M. Larocca, and M. Cerezo, “Theory for equivariant quantum neural networks,” *arXiv preprint arXiv:2210.08566*, 2022.

[19] L. Schatzki, M. Larocca, F. Sauvage, and M. Cerezo, “Theoretical guarantees for permutation-equivariant quantum neural networks,” *arXiv preprint arXiv:2210.09974*, 2022.

[20] A. Pesah, M. Cerezo, S. Wang, T. Volkoff, A. T. Sornborger, and P. J. Coles, “Absence of barren plateaus in quantum convolutional neural networks,” *Physical Review X*, vol. 11, no. 4, p. 041011, 2021.

[21] J. Bausch, “Recurrent quantum neural networks,” *Advances in neural information processing systems*, vol. 33, pp. 1368–1379, 2020.

[22] Y. Takaki, K. Mitarai, M. Negoro, K. Fujii, and M. Kitagawa, “Learning temporal data with a variational quantum recurrent neural network,” *Physical Review A*, vol. 103, no. 5, p. 052414, 2021.

[23] T. J. Elliott, M. Gu, A. J. Garner, and J. Thompson, “Quantum adaptive agents with efficient long-term memories,” *Physical Review X*, vol. 12, no. 1, p. 011007, 2022.

[24] T. J. Elliott, C. Yang, F. C. Binder, A. J. Garner, J. Thompson, and M. Gu, “Extreme dimensionality reduction with quantum modeling,” *Physical Review Letters*, vol. 125, no. 26, p. 260501, 2020.

[25] C. Yang, A. Garner, F. Liu, N. Tischler, J. Thompson, M.-H. Yung, M. Gu, and O. Dahlsten, “Provable superior accuracy in machine learned quantum models,” *arXiv preprint arXiv:2105.14434*, 2021.

[26] J. Chen, H. I. Nurdin, and N. Yamamoto, “Temporal information processing on noisy quantum computers,” *Physical Review Applied*, vol. 14, no. 2, p. 024065, 2020.

[27] S. Y.-C. Chen, D. Fry, A. Deshmukh, V. Rastunkov, and C. Stefanski, “Reservoir computing via quantum recurrent neural networks,” 2022.

[28] L. Banchi, E. Grant, A. Rocchetto, and S. Severini, “Modelling non-markovian quantum processes with recurrent neural networks,” *New Journal of Physics*, vol. 20, no. 12, p. 123030, 2018.

[29] K. Sharma, M. Cerezo, L. Cincio, and P. J. Coles, “Trainability of dissipative perceptron-based quantum neural networks,” *Physical Review Letters*, vol. 128, no. 18, p. 180505, 2022.

[30] D. Heimann, G. Schonhoff, and F. Kirchner, “Learning capability of parametrized quantum circuits,” 2022.

[31] Y. Cao, G. G. Guerreschi, and A. Aspuru-Guzik, “Quantum neuron: an elementary building block for machine learning on quantum computers,” *arXiv preprint arXiv:1711.11240*, 2017.

[32] M. Schuld and F. Petruccione, *Machine learning with quantum computers*. Springer, 2021.

[33] L. Banchi and G. E. Crooks, “Measuring analytic gradients of general quantum evolution with the stochastic parameter shift rule,” *Quantum*, vol. 5, p. 386, 2021.

[34] F. Ciccarello, S. Lorenzo, V. Giovannetti, and G. M. Palma, “Quantum collision models: Open system dynamics from repeated interactions,” *Physics Reports*, vol. 954, pp. 1–70, 2022.

[35] R. J. Williams, “Simple statistical gradient-following algorithms for connectionist reinforcement learning,” *Machine learning*, vol. 8, no. 3, pp. 229–256, 1992.

[36] G. Solomon and L. Weissfeld, “Pseudo maximum likelihood approach for the analysis of multivariate left-censored longitudinal data,” *Statistics in medicine*, vol. 36, no. 1, pp. 81–91, 2017.

[37] P. Virtanen, R. Gommers, T. E. Oliphant, M. Haberland, T. Reddy, D. Cournapeau, E. Burovski, P. Peterson, W. Weckesser, J. Bright, S. J. van der Walt, M. Brett, J. Wilson, K. J. Millman, N. Mayorov, A. R. J. Nelson, E. Jones, R. Kern, E. Larson, C. J. Carey, İ. Polat, Y. Feng, E. W. Moore, J. VanderPlas, D. Laxalde, J. Perktold, R. Cimrman, I. Henriksen, E. A. Quintero, C. R. Harris, A. M. Archibald, A. H. Ribeiro, F. Pedregosa, P. van Mulbregt, and SciPy 1.0 Contributors, “SciPy 1.0: Fundamental Algorithms for Scientific Computing in Python,” *Nature Methods*, vol. 17, pp. 261–272, 2020.

[38] S. Lloyd, M. Schuld, A. Ijaz, J. Izaac, and N. Killoran, “Quantum embeddings for machine learning,” *arXiv preprint arXiv:2001.03622*, 2020.

[39] H.-Y. Huang, M. Broughton, J. Cotler, S. Chen, J. Li, M. Mohseni, H. Neven, R. Babbush, R. Kueng, J. Preskill *et al.*, “Quantum advantage in learning from experiments,” *Science*, vol. 376, no. 6598, pp. 1182–1186, 2022.

[40] S. Meyn, *Control Systems and Reinforcement Learning*. Cambridge University Press, 2022.

[41] A. Peres, *Quantum theory: concepts and methods*. Springer, 1997.